A record of plume-induced plate rotation triggering subduction initiation

Authors: Douwe J.J. van Hinsbergen[1*], Bernhard Steinberger[2,3], Carl Guilmette[4], Marco Maffione[1,5], Derya Gürer[1,6], Kalijn Peters[1], Alexis Plunder[1,7], Peter J. McPhee[1], Carmen Gaina[3], Eldert L. Advokaat[1,5], Reinoud L.M. Vissers[1], and Wim Spakman[1]

Affiliations:

[1]Department of Earth Sciences, Utrecht University, Princetonlaan 8A, 3584 CB Utrecht, Netherlands

[2]GFZ German Research Centre for Geosciences, Potsdam, Germany

[3]Centre of Earth Evolution and Dynamics (CEED), University of Oslo, Norway

[4]Département de Géologie et de Génie Géologique, Université Laval, Québec, QC G1K 7P4, Canada

[5]School of Geography, Earth and Environmental Sciences, University of Birmingham, B15 2TT, UK

[6]School of Earth and Environmental Sciences, University of Queensland, St Lucia, Queensland 4072, Australia

[7]BRGM, F-45060, Orléans, France

*Correspondence to: Douwe J.J. van Hinsbergen (d.j.j.vanhinsbergen@uu.nl)

This manuscript has been accepted for publication in Nature Geoscience on April 22, 2021

The formation of a global network of plate boundaries surrounding a mosaic of lithospheric fragments was a key step in the emergence of Earth's plate tectonics. So far, propositions for plate boundary formation are regional in nature; how plate boundaries are created over thousands of kilometers in geologically short periods remains elusive. Here we show from geological observations that a >12,000 km-long plate boundary formed between the Indian and African plates around 105 Ma. This boundary comprised subduction segments from the eastern Mediterranean region to a newly established India-Africa rotation pole in the west Indian ocean, where it transitioned into a ridge between India and Madagascar. We identify coeval mantle plume rise below Madagascar-India as the only viable trigger of this plate rotation. For this, we provide a proof of concept by torque balance modeling, which reveals that the Indian and African cratonic keels were important in determining plate rotation and subduction initiation in response to the spreading plume head. Our results show that plumes may provide a non-plate-tectonic mechanism for large plate rotation, initiating divergent and convergent plate boundaries far away from the plume head. We suggest that this mechanism may be an underlying cause of the emergence of modern plate tectonics.

The early establishment of plate tectonics on Earth was likely a gradual process that evolved as the cooling planet's lithosphere broke into a mosaic of major fragments, separated by a network of plate boundaries: spreading ridges, transform faults, and subduction zones[1]. The formation of spreading ridges and connecting transform faults is regarded as a passive process, occasionally associated with rising mantle plumes[2]. The formation of subduction zones is less well understood. Explanations for subduction initiation often infer spontaneous gravitational collapse of aging oceanic lithosphere[2], or relocations of subduction zones due to intraplate stress changes in response to arrival of continents, oceanic plateaus, or volcanic arcs in trenches[3]. Mantle plumes have also been suggested as drivers for regional subduction initiation, primarily based on numerical modeling[4-6]. But while such processes may explain how plate tectonics evolves on a regional scale, they do not provide insight into the geodynamic cause(s) for the geologically sudden (<10 My) creation of often long (>1000 km) plate boundaries including new subduction zones[7]. Demonstrating the causes of plate boundary formation involving subduction initiation using the geological record is challenging and requires (i) establishing whether subduction initiation was spontaneous or induced; (ii) if induced, constraining the timing and direction of incipient plate convergence; (iii) reconstructing the entire plate boundary from triple junction to triple junction, as well as the boundaries of neighboring plates, to identify collisions, subduction terminations, or mantle plume arrival that may have caused stress changes driving subduction initiation. In this paper, we provide such an analysis for an intra-oceanic subduction zone that formed within the Neotethys Ocean around 105 Ma ago, to evaluate the driver of subduction initiation and plate boundary formation.

Induced subduction initiation across the Neotethys Ocean

During induced subduction initiation, lower plate burial, dated through prograde mineral growth in rocks of the incipient subduction plate contact, in so-called metamorphic soles[8] predates upper plate extension that is inferred from spreading records in so-called supra-subduction zone (SSZ) ophiolites[8-10,11]. Such SSZ ophiolites have a chemical stratigraphy widely interpreted as having formed at spreading ridges above a nascent subduction zone. Several SSZ ophiolite belts exist in the Alpine-Himalayan mountain belt, which formed during the closure of the Neotethys Ocean[12,13] (Fig. 1A). One of these ophiolite belts formed in Cretaceous time and runs from the eastern Mediterranean region, along northern Arabia, to Pakistan. Incipient lower plate burial has been dated through Lu/Hf prograde garnet growth ages of ~104 Ma in metamorphic soles in Oman as well as in the eastern Mediterranean region[8,14]. Upper plate extension and SSZ ophiolite spreading has been dated using magmatic zircon U/Pb ages and synchronous metamorphic sole ^{40}Ar/^{39}Ar cooling ages and occurred at 96-95 Ma (Pakistan, Oman)[15,16] to 92-90 Ma (Iran, eastern Mediterranean region)[17]. The 8-14 Myr time delay between initial lower plate burial and upper plate extension demonstrates that subduction initiation was induced[8].

An initial ~E-W convergence direction at this subduction zone was constrained through paleomagnetic analysis and detailed kinematic reconstruction of post-subduction initiation deformation of the eastern Mediterranean region, Oman, and Pakistan, and was accommodated at ~N-S striking trench segments[13,18-20]. This is surprising: for hundreds of Ma and throughout the Tethyan realm, rifts and ridges accommodated the separation of continental fragments off northern Gondwana in the south and their accretion to the southern Eurasian margin at subduction zones in the north[21,22]. The ~E-W convergence that triggered ~105 Ma subduction initiation across the Neotethys ocean was thus near orthogonal to the long-standing plate motions. To find the trigger inducing this subduction, we developed the first comprehensive reconstruction of the entire ~12,000 km long plate boundary that formed at ~105 Ma and placed this in context of reconstructions of collisions and mantle plumes of the Neotethyan realm (Fig. 1).

Geological reconstruction of incipient plate boundary

The SSZ ophiolites that formed at the juvenile Cretaceous intra-Neotethyan subduction zone are now found as klippen on intensely deformed accretionary orogenic belts (Fig. 1A) that formed when the continents of Greater Adria, Arabia, and India arrived in subduction zones. We reconstructed these orogenic belts (Fig. 1) and restored these continents, and the Cretaceous ophiolites that were thrust upon these, into their configuration at 105 Ma (Fig. 1C) (see Methods).

The westernmost geological record of the Cretaceous intra-Neotethyan subduction zone is found in eastern Greece and western Turkey, where it ended in a trench-trench-trench triple junction with subduction zones along the southern Eurasian margin[18]. From there, east-dipping (in the west) and west-dipping (in the east) subduction segments followed the saw-toothed shape of the Greater Adriatic and Arabian continental margins (Fig. 1C) and initiated close to it: rocks of these continental margins already underthrusted the ophiolites within 5-15 My after SSZ ophiolite spreading[14,23,24], and continent-derived zircons have been found in metamorphic sole rocks[25]. Subduction segments likely nucleated along ancient N-S and NE-SW trending fracture zones and linked through highly oblique, north-dipping subduction zones that trended parallel to and likely reactivated the pre-existing (hyper)extended passive margins (Fig. 1B, C)[20,23]. Subducted remnants of the Cretaceous intra-Neotethyan subduction are well-resolved in the present-day mantle as slabs in the mid-mantle below the southeastern Mediterranean Sea, central Arabia and the west Indian Ocean[26].

East of Arabia, we trace the intra-oceanic plate boundary to a NE-SW striking, NW-dipping subduction zone between the Kabul Block and the west Indian passive margin. The 96 Ma Waziristan ophiolites of Pakistan formed above this subduction zone, perhaps by inverting an Early Cretaceous spreading ridge between the Kabul Block and India[13] and were thrust eastward onto the Indian margin[13,16] (Fig. 1B, C). The Cretaceous intra-Neotethyan plate boundary may have been convergent to the Amirante Ridge in the west Indian Ocean[13], from where it became extensional instead and developed a rift, and later a spreading ridge, in the Mascarene Basin that accommodated separation of India from Madagascar[13,27,28] (Fig. 1B). The plate boundary ended in a ridge-ridge-ridge triple junction in the south Indian Ocean[13,28] (Fig. 1B).

The newly formed Cretaceous plate boundary essentially temporarily merged a large part of Neotethyan oceanic lithosphere between Arabia and Eurasia to the Indian plate. This plate was >12,000 km long from triple junction to triple junction, and reached from 45°S to 45°N, with 4500 km of rift/ridge in the southeast and 7500 km of subduction zone in the northwest and with a transition between the convergent and divergent segments, representing the India-Africa Euler pole[13], in the west Indian Ocean, at a latitude between Pakistan and the Amirante Ridge (Fig. 1B). Marine geophysical constraints show a ~4° counterclockwise rotation of India relative to Africa about the west Indian Ocean Euler pole during rifting preceding the ~83 Ma onset of oceanic spreading in the Mascarene Basin[27-29], associated with up to hundreds of km of ~E-W convergence across the Neotethys (Fig. 1D).

The neighboring plates of the intra-Neotethyan subduction zone at 105 Ma were thus Africa and India. The African plate was mostly surrounded by ridges and had a complex subduction plate boundary in the Mediterranean region[30]. The Indian plate was surrounded by ridge-transform systems in the south and east and by subduction in the north, and may have contained rifts and ridges between the Indian continent and Eurasia[13,28]. The Neotethys lithosphere between Arabia-Greater Adria and Eurasia continued unbroken to the north-dipping subduction zone that had already existed along the southern Eurasian margin since the Jurassic[31,32]: the spreading ridges that existed during Neotethys Ocean opening in the Permian-Triassic (north of Arabia)[33], and Triassic-Jurassic (eastern Mediterranean region)[23] had already subducted below Eurasia before 105 Ma[19,33] (Fig. 1B, C).

Identifying potential drivers of subduction initiation

Candidate processes to trigger the reconstructed plate boundary formation at 105 Ma are terminations of existing subduction zones by arrival of buoyant lithosphere or the rise of mantle plumes. Southern Eurasia contains relics of many microcontinents that accreted at or clogged subduction zones since the Paleozoic, but none of these events started or ended around 105 Ma[13,21-23,33-35]. Continental subduction and collision was ongoing in the central Mediterranean region[23], but it is not evident how this or any other changes in subduction dynamics along the E-W trending southern Eurasian margin would lead to E-W convergence in the Neotethys Ocean. In the eastern Neotethys, a mid-Cretaceous collision of the intra-oceanic Woyla Arc with the Sundaland continental margin led to a subduction polarity reversal initiating eastward subduction below Sundaland[36], which is recorded in ophiolites on the Andaman Islands. There, metamorphic sole rocks with ^{40}Ar/^{39}Ar hornblende cooling ages of 105-106 Ma, and likely coeval SSZ ophiolite spreading ages[37] reveal that this subduction zone may have developed slab pull around the same time as the Indian Ocean-western Neotethys plate boundary formed (Fig 1C). However, eastward slab pull below Sundaland cannot drive E-W convergence in the Neotethys to the west, and Andaman SSZ extension may well be an expression rather than the trigger of Indian plate rotation. We find no viable plate tectonics-related driver of the ~105 Ma plate boundary formation that we reconstructed here.

A key role, however, is possible for the only remaining geodynamic, non-plate-tectonic, plate-motion driver in the region: a mantle plume. India-Madagascar continental breakup is widely viewed[13,27,37] as related to the ~94 Ma and younger formation of the Morondava Large Igneous Province (LIP) on Madagascar[38] and southwest India[39]. This LIP, however, started forming ~10 Ma after initial plate boundary formation. To understand whether the plume may be responsible for both LIP emplacement and plate boundary formation, we explore existing numerical models of plume-plate interaction and conduct explorative torque-balance simulations of plume-lithosphere interaction.

Mantle plumes driving subduction initiation

Numerical simulations of plume-lithosphere interaction have already identified that plume head spreading below the lithosphere leads to horizontal asthenospheric flow that exerts a ‘plume push’ force on the base of the lithosphere, particularly in the presence of a cratonic keel[5,40,41]. Plume push may accelerate plates by several cm/yr[41] and has been proposed as a potential driver of subduction initiation[5].

In many cases, including in the case of the Morondava LIP, LIP eruption and emplacement shortly preceded continental breakup, but pre-break up rifting preceded LIP emplacement by 10-15 Myr[27]. This early rifting typically is interpreted to indicate that the plume migrated along the base of the lithosphere into a pre-existing rift that formed independently of plume rise[27]. However, in numerical simulations dynamic uplift[42] and plume push[41] already start to accelerate plates 10-15 Myr before the plume head reaches the base of the lithosphere and emplaces the LIP. Numerical simulations thus predict the observed delay between plume push, as a driver for early rifting and subduction initiation, and LIP eruption and emplacement.

Here, we add to these plume-lithosphere coupling experiments by conducting proof-of-concept torque-balance simulations particularly exploring why the observed India-Africa Euler pole is so close to the plume head such that the associated plate rotation between Africa and India caused E-W convergence in the Neotethys. We performed semi-analytical computations, including both the Indian and African plates at ~105 Ma, and assess the influence of cratonic keels on the position of the India-Africa Euler pole (Fig. 2, see Methods).

In our computations without cratonic keels, plume push under Madagascar/India caused counterclockwise rotation of India versus Africa, but about an Euler pole situated far north of Arabia, (Fig. 2A) without inducing significant E-W convergence within the Neotethys. However, in experiments that include keels of the Indian and African cratonic lithosphere, which are strongly coupled to the sub-asthenospheric mantle, the computed Euler pole location is shifted southward towards the Indian continent, inducing E-W convergence along a larger part of the plate boundary within the Neotethys Ocean (Fig. 2B).

Convergence of up to several hundreds of km, sufficient to induce self-sustaining subduction[27], is obtained if plume material is fed into – and induced flow is confined to – a 200 km thick weak asthenospheric layer. The thinner this layer is, the further the plume head spreads, and pushes the plate. The modern Indian cratonic root used in our computations has likely eroded considerably during interaction with the ~70-65 Ma Deccan plume[43]. India may have had a thicker and/or laterally more extensive cratonic root at ~105 Ma than modeled here which would further enhance coupling of the lithosphere and the sub-asthenospheric mantle. Furthermore, an Euler pole close to India and a long convergent boundary to the north requires much weaker coupling in the northern (oceanic) part of the India plate (Fig. 2). In this case, results remain similar as long as the plume impinges near the southern part of the western boundary of continental India.

An order of magnitude estimate of the maximum plume-induced stresses, assuming no frictional resistance at other plate boundaries, is obtained from the rising force of $\sim 1.5 \cdot 10^{20}$ N of a plume head with 1000 km diameter and density contrast 30 kg/m^3. If half of this force acts on the India plate and with a lever arm of 4000 km, this corresponds to a torque of $3 \cdot 10^{26}$ Nm. Once, at the onset of rifting, ridge push is established as an additional force in the vicinity of the plume, we estimate that this number may increase by up to a few tens of per cent. This torque can be balanced at the convergent boundary (length ~5000 km, plate thickness ~100 km) involving stresses of ~240 MPa, much larger than estimates of frictional resistance between subducting and overriding plates that are only of the order of tens of MPa[44]. For this estimate, we neglect any frictional resistance at the base of the plate and at any other plate boundary – essentially considering the plate as freely rotating above a pinning point. This is another endmember scenario, as opposed to our above convergence estimate, where we had considered friction at the plate base but neglected it at all plate boundaries. Therefore, the estimate of 240 MPa may be considered as an upper bound but being compressive and oriented in the right direction it shows the possibility of subduction initiation as has occurred in reality along the likely weakened passive margin region of Arabia and Greater Adria. Moreover, the plume-induced compressive stresses may have added to pre-existing compressive stresses, in particular due to ridge-push around the African and Indian plates. Such additional compressive stresses may contribute to shifting the Euler pole further south, closer to the position reconstructed in Fig. 1.

Subduction became self-sustained ~8-12 Ma after its initiation, as marked by the 96-92 Ma age of SSZ spreading[15,17]: inception of this spreading shows that subduction rates exceeded convergence rates, and reconstructed SSZ spreading rates were an order of magnitude higher[15] than Africa-Arabia or Indian absolute plate motions[41,45] signaling slab roll-back, i.e. self-sustained subduction[20,46]. Numerical models suggest that self-sustained subduction may start after ~50-100 km of induced convergence[7], corresponding to ~1° of India-Africa rotation between ~105 and ~96-92 Ma. Subsequent east and west-dipping subduction segments (Fig. 1) may have contributed to and accelerated the India-Africa/Arabia rotation, driving the propagation of the Euler pole farther to the south (compare Fig. 2A, C).

Mantle plumes as an initiator of plate tectonics?

Previously, numerical modeling has shown that mantle plumes may trigger circular subduction initiation around a plume head[4], where local plume-related convection may drive subduction of thermally weakened lithosphere. This subduction would propagate through slab roll-back and may have started the first subduction features on Earth[4]. 3D convective models do produce a global network of plate boundaries[47,48]but the role of plumes in initiating new subduction zones within this network is unclear. Here, we have provided the first evidence that plume rise formed a >12,000 km long plate boundary composed of both convergent and divergent segments. Our documented example is Cretaceous in age but geological observations showing a general temporal overlap between LIP emplacement and formation of SSZ ophiolite belts over more than a billion years[49] suggest that plume rise is a key driving factor in the formation of subduction plate boundaries. Because mantle plumes are thought to be also common features on planets without plate tectonics, such as Mars and Venus[50], they may have played a vital role in the emergence of modern style plate tectonics on Earth. That plumes may have been key for the evolution of plate tectonics on Earth, as we suggest, but apparently insufficient on Mars and Venus, provides a new outlook on understanding the different planetary evolutions.

References:

1 Lenardic, A. The diversity of tectonic modes and thoughts about transitions between them. *Philosophical Transactions of the Royal Society A: Mathematical, Physical and Engineering Sciences* **376**, 20170416 (2018).

2 Stern, R. J. Subduction initiation: spontaneous and induced. *Earth and Planetary Science Letters* **226**, 275-292, doi:10.1016/s0012-821x(04)00498-4 (2004).

3 Hall, C. E., Gurnis, M., Sdrolias, M., Lavier, L. L. & Müller, R. D. Catastrophic initiation of subduction following forced convergence across fracture zones. *Earth and Planetary Science Letters* **212**, 15-30, doi:10.1016/s0012-821x(03)00242-5 (2003).

4 Gerya, T. V., Stern, R. J., Baes, M., Sobolev, S. V. & Whattam, S. A. Plate tectonics on the Earth triggered by plume-induced subduction initiation. *Nature* **527**, 221-225, doi:10.1038/nature15752 (2015).

5 Pusok, A. E. & Stegman, D. R. The convergence history of India-Eurasia records multiple subduction dynamics processes. *Science Advances* **6**, eaaz8681 (2020).

6 Baes, M., Sobolev, S., Gerya, T. & Brune, S. Plume-Induced Subduction Initiation: Single-Slab or Multi-Slab Subduction? *Geochemistry, Geophysics, Geosystems* **21**, e2019GC008663 (2020).

7 Gurnis, M., Hall, C. & Lavier, L. Evolving force balance during incipient subduction. *Geochemistry, Geophysics, Geosystems* **5**, doi:10.1029/2003gc000681 (2004).

8 Guilmette, C. *et al.* Forced subduction initiation recorded in the sole and crust of the Semail Ophiolite of Oman. *Nature Geoscience* **11**, 688-695 (2018).

9 Stern, R. J. & Gerya, T. Subduction initiation in nature and models: A review. *Tectonophysics*, doi:10.1016/j.tecto.2017.10.014 (2017).

10 Agard, P. *et al.* Plate interface rheological switches during subduction infancy: Control on slab penetration and metamorphic sole formation. *Earth and Planetary Science Letters* **451**, 208-220 (2016).

11 van Hinsbergen, D. J. J. *et al.* Dynamics of intraoceanic subduction initiation: 2. Suprasubduction zone ophiolite formation and metamorphic sole exhumation in context of absolute plate motions. *Geochemistry, Geophysics, Geosystems* **16**, 1771-1785, doi:10.1002/2015gc005745 (2015).

12 Dilek, Y. & Furnes, H. Ophiolite genesis and global tectonics: Geochemical and tectonic fingerprinting of ancient oceanic lithosphere. *Geological Society of America Bulletin* **123**, 387-411, doi:10.1130/b30446.1 (2011).

13 Gaina, C., van Hinsbergen, D. J. J. & Spakman, W. Tectonic interactions between India and Arabia since the Jurassic reconstructed from marine geophysics, ophiolite geology, and seismic tomography. *Tectonics* **34**, 875-906, doi:10.1002/2014tc003780 (2015).

14 Pourteau, A. *et al.* Thermal evolution of an ancient subduction interface revealed by Lu–Hf garnet geochronology, Halilbağı Complex (Anatolia). *Geoscience Frontiers* **10**, 127-148, doi:10.1016/j.gsf.2018.03.004 (2019).

15 Rioux, M. *et al.* Synchronous formation of the metamorphic sole and igneous crust of the Semail ophiolite: New constraints on the tectonic evolution during ophiolite formation from high-precision U–Pb zircon geochronology. *Earth and Planetary Science Letters* **451**, 185-195 (2016).

16 Robinson, J., Beck, R., Gnos, E. & Vincent, R. K. New structural and stratigraphic insights for northwestern Pakistan from field and Landsat Thematic Mapper data. *Geological Society of America Bulletin* **112**, 364-374, doi:10.1130/0016-7606(2000)112<364:Nsasif>2.0.Co;2 (2000).

17 Parlak, O. The tauride ophiolites of Anatolia (Turkey): A review. *Journal of Earth Science* **27**, 901-934, doi:10.1007/s12583-016-0679-3 (2016).

18 van Hinsbergen, D. J. J. *et al.* Tectonic evolution and paleogeography of the Kırşehir Block and the Central Anatolian Ophiolites, Turkey. *Tectonics* **35**, 983-1014, doi:10.1002/ (2016).

19 Maffione, M., van Hinsbergen, D. J. J., de Gelder, G. I. N. O., van der Goes, F. C. & Morris, A. Kinematics of Late Cretaceous subduction initiation in the Neo-Tethys Ocean reconstructed from ophiolites of Turkey, Cyprus, and Syria. *Journal of Geophysical Research: Solid Earth* **122**, 3953-3976, doi:10.1002/2016jb013821 (2017).

20 van Hinsbergen, D. J., Maffione, M., Koornneef, L. M. & Guilmette, C. Kinematic and paleomagnetic restoration of the Semail ophiolite (Oman) reveals subduction initiation along an ancient Neotethyan fracture zone. *Earth and Planetary Science Letters* **518**, 183-196 (2019).

21 Torsvik, T. H. & Cocks, L. R. M. *Earth history and palaeogeography*. 317 (Cambridge University Press, 2017).

22 Wan, B. *et al.* Cyclical one-way continental rupture-drift in the Tethyan evolution: Subduction-driven plate tectonics. *Science China Earth Sciences*, 1-12 (2019).

23 van Hinsbergen, D. J. J. *et al.* Orogenic architecture of the Mediterranean region and kinematic reconstruction of its tectonic evolution since the Triassic. *Gondwana Research* **81**, 79-229 (2020).

24 Warren, C. J., Parrish, R. R., Waters, D. J. & Searle, M. P. Dating the geologic history of Oman's Semail ophiolite: insights from U-Pb geochronology. *Contributions to Mineralogy and Petrology* **150**, 403-422, doi:10.1007/s00410-005-0028-5 (2005).

25 Güngör, T. *et al.* Kinematics and U-Pb zircon ages of the sole metamorphics of the Marmaris Ophiolite, Lycian Nappes, Southwest Turkey. *International Geology Review* **61**, 1124-1142 (2019).

26 van der Meer, D. G., van Hinsbergen, D. J. J. & Spakman, W. Atlas of the underworld: Slab remnants in the mantle, their sinking history, and a new outlook on lower mantle viscosity. *Tectonophysics* **723**, 309-448, doi:10.1016/j.tecto.2017.10.004 (2018).

27 Buiter, S. J. & Torsvik, T. H. A review of Wilson Cycle plate margins: A role for mantle plumes in continental break-up along sutures? *Gondwana Research* **26**, 627-653 (2014).

28 Gibbons, A. D., Whittaker, J. M. & Müller, R. D. The breakup of East Gondwana: Assimilating constraints from Cretaceous ocean basins around India into a best-fit tectonic model. *Journal of Geophysical Research: Solid Earth* **118**, 808-822, doi:10.1002/jgrb.50079 (2013).

29 Gaina, C., Müller, R. D., Brown, B., Ishihara, T. & Ivanov, S. Breakup and early seafloor spreading between India and Antarctica. *Geophysical Journal International* **170**, 151-169, doi:10.1111/j.1365-246X.2007.03450.x (2007).

30 Gaina, C. *et al.* The African Plate: A history of oceanic crust accretion and subduction since the Jurassic. *Tectonophysics* **604**, 4-25, doi:10.1016/j.tecto.2013.05.037 (2013).

31 Agard, P., Jolivet, L., Vrielynck, B., Burov, E. & Monié, P. Plate acceleration: The obduction trigger? *Earth and Planetary Science Letters* **258**, 428-441, doi:10.1016/j.epsl.2007.04.002 (2007).

32 Jolivet, L. *et al.* Neo-Tethys geodynamics and mantle convection: from extension to compression in Africa and a conceptual model for obduction. *Canadian journal of earth sciences* **53**, 1190-1204 (2015).

33 Stampfli, G. M. & Borel, G. A plate tectonic model for the Paleozoic and Mesozoic constrained by dynamic plate boundaries and restored synthetic oceanic isochrons. *Earth and Planetary Science Letters* **196**, 17-33 (2002).

34 van Hinsbergen, D. J. J. *et al.* Reconstructing Greater India: Paleogeographic, kinematic, and geodynamic perspectives. *Tectonophysics* **760**, 69-94, doi:10.1016/j.tecto.2018.04.006 (2019).

35 Kapp, P. & DeCelles, P. G. Mesozoic–Cenozoic geological evolution of the Himalayan-Tibetan orogen and working tectonic hypotheses. *American Journal of Science* **319**, 159-254 (2019).

36 Advokaat, E. L. *et al.* Early Cretaceous origin of the Woyla Arc (Sumatra, Indonesia) on the Australian plate. *Earth and Planetary Science Letters* **498**, 348-361 (2018).

37 Plunder, A. *et al.* History of subduction polarity reversal during arc-continent collision: constraints from the Andaman Ophiolite and its metamorphic sole. *Tectonics*, e2019TC005762 (2020).

38 Torsvik, T. *et al.* Late Cretaceous magmatism in Madagascar: palaeomagnetic evidence for a stationary Marion hotspot. *Earth and Planetary Science Letters* **164**, 221-232 (1998).

39 Mohan, M. R. *et al.* The Ezhimala igneous complex, southern India: Possible imprint of late Cretaceous magmatism within rift setting associated with India–Madagascar separation. *Journal of Asian Earth Sciences* **121**, 56-71 (2016).

40 Cande, S. C. & Stegman, D. R. Indian and African plate motions driven by the push force of the Reunion plume head. *Nature* **475**, 47-52, doi:10.1038/nature10174 (2011).

41 van Hinsbergen, D. J. J., Steinberger, B., Doubrovine, P. V. & Gassmöller, R. Acceleration and deceleration of India-Asia convergence since the Cretaceous: Roles of mantle plumes and continental collision. *Journal of Geophysical Research* **116**, doi:10.1029/2010jb008051 (2011).

42 Wang, Y. & Li, M. The interaction between mantle plumes and lithosphere and its surface expressions: 3-D numerical modelling. *Geophysical Journal International*, doi:10.1093/gji/ggab014 (2021).

43 Kumar, P. *et al.* The rapid drift of the Indian tectonic plate. *Nature* **449**, 894-897, doi:10.1038/nature06214 (2007).

44 Lamb, S. & Davis, P. Cenozoic climate change as a possible cause for the rise of the Andes. *Nature* **425**, 792-797 (2003).

45 van der Meer, D. G., Spakman, W., van Hinsbergen, D. J. J., Amaru, M. L. & Torsvik, T. H. Towards absolute plate motions constrained by lower-mantle slab remnants. *Nature Geoscience* **3**, 36-40, doi:10.1038/ngeo708 (2010).

46 Tavani, S., Corradetti, A., Sabbatino, M., Seers, T. & Mazzoli, S. Geological record of the transition from induced to self-sustained subduction in the Oman Mountains. *Journal of Geodynamics* **133**, 101674 (2020).

47 Tackley, P. J. Mantle convection and plate tectonics: Toward an integrated physical and chemical theory. *Science* **288**, 2002-2007 (2000).

48 Coltice, N., Husson, L., Faccenna, C. & Arnould, M. What drives tectonic plates? *Science Advances* **5**, eaax4295 (2019).

49 Dilek, Y. Ophiolite pulses, mantle plumes and orogeny. *Geological Society, London, Special Publications* **218**, 9-19 (2003).

50 Ernst, R., Grosfils, E. & Mege, D. Giant dike swarms: Earth, venus, and mars. *Annual Review of Earth and Planetary Sciences* **29**, 489-534 (2001).

51 Müller, R. D. *et al.* GPlates: building a virtual Earth through deep time. *Geochemistry, Geophysics, Geosystems* **19**, 2243-2261 (2018).

52 Clube, T. M. M., Creer, K. M. & Robertson, A. H. F. Palaeorotation of the Troodos microplate, Cyprus. *Nature* **317**, 522, doi:10.1038/317522a0 (1985).

53 Morris, A., Meyer, M., Anderson, M. W. & MacLeod, C. J. Clockwise rotation of the entire Oman ophiolite occurred in a suprasubduction zone setting. *Geology* **44**, 1055-1058 (2016).

54 McQuarrie, N. & van Hinsbergen, D. J. J. Retrodeforming the Arabia-Eurasia collision zone: Age of collision versus magnitude of continental subduction. *Geology* **41**, 315-318, doi:10.1130/g33591.1 (2013).

55 Monsef, I. *et al.* Evidence for an early-MORB to fore-arc evolution within the Zagros suture zone: Constraints from zircon U-Pb geochronology and geochemistry of the Neyriz ophiolite (South Iran). *Gondwana Research* **62**, 287-305 (2018).

56 Galoyan, G. *et al.* Geology, geochemistry and 40Ar/39Ar dating of Sevan ophiolites (Lesser Caucasus, Armenia): evidence for Jurassic Back-arc opening and hot spot event between the South Armenian Block and Eurasia. *Journal of Asian Earth Sciences* **34**, 135-153 (2009).

57 Çelik, Ö. F. *et al.* Jurassic metabasic rocks in the Kızılırmak accretionary complex (Kargı region, Central Pontides, Northern Turkey). *Tectonophysics* **672-673**, 34-49, doi:10.1016/j.tecto.2016.01.043 (2016).

58 Topuz, G. *et al.* Jurassic ophiolite formation and emplacement as backstop to a subduction-accretion complex in northeast Turkey, the Refahiye ophiolite, and relation to the Balkan ophiolites. *American Journal of Science* **313**, 1054-1087, doi:10.2475/10.2013.04 (2014).

59 Ao, S. *et al.* U–Pb zircon ages, field geology and geochemistry of the Kermanshah ophiolite (Iran): From continental rifting at 79Ma to oceanic core complex at ca. 36Ma in the southern Neo-Tethys. *Gondwana Research* **31**, 305-318, doi:10.1016/j.gr.2015.01.014 (2016).

60 Peters, T. & Mercolli, I. Extremely thin oceanic crust in the Proto-Indian Ocean: Evidence from the Masirah Ophiolite, Sultanate of Oman. *Journal of Geophysical Research: Solid Earth* **103**, 677-689, doi:10.1029/97jb02674 (1998).

61 Gnos, E. *et al.* Bela oceanic lithosphere assemblage and its relation to the Reunion hotspot. *Terra Nova* **10**, 90-95 (1998).

62 Tapponnier, P., Mattauer, M., Proust, F. & Cassaigneau, C. Mesozoic ophiolites, sutures, and arge-scale tectonic movements in Afghanistan. *Earth and Planetary Science Letters* **52**, 355-371 (1981).

63 van Hinsbergen, D. J. J. *et al.* Greater India Basin hypothesis and a two-stage Cenozoic collision between India and Asia. *Proc Natl Acad Sci U S A* **109**, 7659-7664, doi:10.1073/pnas.1117262109 (2012).

64 Yuan, J. *et al.* Rapid drift of the Tethyan Himalaya terrane before two-stage India-Asia collision. *National Science Review* (2020).

65 Hébert, R. *et al.* The Indus–Yarlung Zangbo ophiolites from Nanga Parbat to Namche Barwa syntaxes, southern Tibet: First synthesis of petrology, geochemistry, and geochronology with incidences on geodynamic reconstructions of Neo-Tethys. *Gondwana Research* **22**, 377-397, doi:10.1016/j.gr.2011.10.013 (2012).

66 Zahirovic, S. *et al.* Tectonic evolution and deep mantle structure of the eastern Tethys since the latest Jurassic. *Earth-Science Reviews* **162**, 293-337 (2016).

67 Huang, W. *et al.* Lower Cretaceous Xigaze ophiolites formed in the Gangdese forearc: Evidence from paleomagnetism, sediment provenance, and stratigraphy. *Earth and Planetary Science Letters* **415**, 142-153, doi:10.1016/j.epsl.2015.01.032 (2015).

68 Westerweel, J. *et al.* Burma Terrane part of the Trans-Tethyan arc during collision with India according to palaeomagnetic data. *Nature Geoscience* **12**, 863-868 (2019).

69 Jagoutz, O., Royden, L., Holt, A. F. & Becker, T. W. Anomalously fast convergence of India and Eurasia caused by double subduction. *Nature Geoscience* **8**, 475-478, doi:10.1038/ngeo2418 (2015).

70 Höink, T. & Lenardic, A. Long wavelength convection, Poiseuille–Couette flow in the low-viscosity asthenosphere and the strength of plate margins. *Geophysical Journal International* **180**, 23-33 (2010).

71 Höink, T., Jellinek, A. M. & Lenardic, A. Viscous coupling at the lithosphere-asthenosphere boundary. *Geochemistry, Geophysics, Geosystems* **12** (2011).

72 Campbell, I. H. Testing the plume theory. *Chemical Geology* **241**, 153-176 (2007).

73 Doubrovine, P. V., Steinberger, B. & Torsvik, T. H. A failure to reject: Testing the correlation between large igneous provinces and deep mantle structures with EDF statistics. *Geochemistry, Geophysics, Geosystems* **17**, 1130-1163 (2016).

74 Steinberger, B. Topography caused by mantle density variations: observation-based estimates and models derived from tomography and lithosphere thickness. *Geophysical Journal International* **205**, 604-621 (2016).

75 Steinberger, B. & Becker, T. W. A comparison of lithospheric thickness models. *Tectonophysics* **746**, 325-338 (2018).

Corresponding author: Douwe van Hinsbergen (d.j.j.vanhinsbergen@uu.nl)

Acknowledgments: DJJvH acknowledges funding through European Research Council Starting Grant 306810 (SINK) (also funding MM, DG, AP, and ELA) Netherlands Organization for Scientific Research (NWO) Vidi grant 864.11.004 (also funding KP and PJmcP) and Netherlands Organization for Scientific Research (NWO) Vici grant 865.17.001. BS and CGa received funding from the Research Council of Norway through its Centres of Excellence funding scheme, project number 223272. BS acknowledges the innovation pool of the Helmholtz Association through the "Advanced Earth System Modelling Capacity (ESM)" activity. CG was funded through Discovery Grant (RGPIN-2014-05681) from the National Science and Engineering Research Council of Canada. We thank Inge Loes ten Kate and Debaditya Bandyopadhyay for discussion, and Fabio Capitanio and Dietmar Müller for reviews.

Author contributions: DJJvH, BS, WS designed research. DJJvH, CGu, MM, DG, KP, AP, PJmcP, CGa, ELA and RLMV developed the kinematic reconstruction; BS performed modelling; DJJvH, BS, CGu, WS wrote the paper, all authors made corrections and edits.

Competing interests: All authors declare no competing interests.

Fig. 1. **Plate kinematic reconstructions of the Neotethys Ocean and surrounding continents.** a) the present-day; b) 70 Ma; c) 105 Ma, corresponding to the timing of intra-Neotethyan subduction initiation and d) 110 Ma, just before intra-Neotethyan subduction initiation. See Methods for the plate reconstruction approach and sources of detailed restorations. Reconstructions show in a mantle reference frame[45]. AR = Amirante Ridge; Emed = Eastern Mediterranean Region; Ir = Iran; LIP = Large Igneous Province; Mad = Madagascar; Mas = Mascarene Basin; Pak = Pakistan, Tur = Turkey; Waz = Waziristan Ophiolite.

Fig. 2. Torque balance modeling results of plumes affecting plates similar to India and Africa with, and without cratonic keels. The computed total displacement, induced by the Morondava plume (pink circle) for the restored ~105 Ma plate configuration (Fig. 1c) for plates without (a, b) and with (c, d) African and Indian cratonic keels, in an Africa-fixed (a, c), or mantle reference frame[45] (b, d) (see Methods). Ten degree grid spacing; locations of plates, lithosphere thickness and the plume are reconstructed in a slab-fitted mantle reference frame[45].

Methods: *Kinematic reconstruction* – The kinematic restoration of Neotethyan intra-oceanic subduction was made in GPlates plate reconstruction software (www.gplates.org)[51]. First, we systematically restored stable plates using marine geophysical data from the Atlantic and Indian Ocean, and then restored continental margin deformation that occurred following the arrival of continental lithosphere below the oceanic lithosphere preserved as ophiolites. These restorations are based on a systematic reconstruction protocol, based on magnetic anomalies and fracture zones of present-day sea floor and geophysical constraints on pre-drift extension in adjacent passive continental margins[23], followed by kinematic restoration of post-obduction orogenic deformation using structural geological constraints on continental extension, strike-slip deformation, and shortening, and paleomagnetic constraints on vertical axis rotations. We then restored pre-emplacement vertical axis microplate rotations[52,53], as well as paleo-orientations of the SSZ spreading ridges at which the ophiolitic crust formed[18-20]. The reconstruction shown in Fig. 1B compiles kinematic restorations for the eastern Mediterranean region[23], Iran[54], Oman[20], Pakistan[13], and the Himalaya[34]. Ophiolites interpreted to be part of the Cretaceous subduction system include the 96-90 Ma, Cretaceous ophiolites exposed in SE Greece, Anatolia, Cyprus, Syria, and Iraq, the Neyriz ophiolite of Iran, the Semail ophiolite in Oman, and the Waziristan-Khost ophiolite in Pakistan and Afghanistan[15-17,55]. The Jurassic ophiolite belts of northern Turkey and Armenia[56-58] and the late Cretaceous (<80 Ma) Kermanshah ophiolite of Iran[59] are not included and are instead interpreted to have formed along the southern Eurasian margin[23]. The Masirah Ophiolite of East Oman[60] and the uppermost Cretaceous Bela, Muslim Bagh, and Kabul-Altimur ophiolites of Pakistan and Afghanistan[61,62] are interpreted to reflect oblique latest Cretaceous to Paleogene India-Arabia convergence[13] and are also unrelated to the event studied here. Restoration of intra-oceanic subduction prior to the arrival of the continental margins used paleomagnetic data from the ophiolites of Oman, Syria, Cyprus, and Turkey that constrain vertical axis rotations, as well as the orientation of sheeted dyke following cooling after intrusion[18-20,52,53] as proxy for original ridge and intra-oceanic trench orientations. These paleomagnetic data systematically revealed N-S to NW-SE primary sheeted dyke orientations[18-20,52,53]. Because the ages of the SSZ ophiolites in the Neotethyan belt do not laterally progress, spreading must have occurred near-orthogonal to the associated trench, which must thus also have been striking N-S to NE-SW, as shown in the reconstruction of Fig. 1.

How far the Indian plate continued northwards around 105 Ma is subject to ongoing debate. On the one hand, the northern Indian continental margin has been proposed to have rifted off India sometime in the Cretaceous[34,63], but recent paleomagnetic data suggest that this process occurred in the late Cretaceous, well after 100 Ma[64]. Others inferred that the north Indian continent had a passive margin contiguous with oceanic Neotethyan lithosphere since the middle Jurassic or before and continued to a subduction zone below the SSZ ophiolites found in the Himalayan suture zone and the Kohistan arc[35,65,66]. Sedimentary and paleomagnetic data demonstrate that these ophiolites formed adjacent to the Eurasian margin in the Early Cretaceous[67], although they may have migrated southward during slab roll-back in the Late Cretaceous[35]. Recent paleomagnetic data have shown that a subduction zone may have existed within the Neotethys to the west of the Andaman Islands, above which the West Burma Block would have been located (Figure 1)[68]. Our reconstruction of the eastern Neotethys may thus be oversimplified. However, the geological record of the West Burma Block shows that this subduction zone already existed as early as 130 Ma, and E-W trending until well into the Cenozoic[68], and we see no reason to infer that changes in the eastern Neotethys contributed to the plate boundary formation discussed here. Some have speculated that the West Burma subduction zone would have been connected to a long-lived, equatorial subduction zone within the Neotethys all along the Indian segment that would already have existed in the Early Cretaceous[69]: this scenario remains unconstrained by paleomagnetic data, and is inconsistent with sediment provenance data from the Himalaya and overlying ophiolites[35]. In summary, the Indian plate around 105 Ma continued far into the Neotethyan realm, and the India-Africa rotation is a likely driver of E-W convergence sparking subduction initiation close to the northern Gondwana margin purported in Figure 1.

Torque balance modeling – Forces considered here include (i) the push due to plume-induced flow in the asthenosphere and (ii) the drag due to shear flow between the moving plate and a deeper mantle at rest (Fig. S1). In the first case, we disregard any lateral variations. Plume-induced flow is treated as Poiseuille flow, i.e. with parabolic flow profile, in an asthenospheric channel of thickness h_c, radially away from the plume stem. Since at greater distance plume-induced flow will eventually not remain confined to the asthenosphere, we only consider it to a distance 2400 km, in accord with numerical results[41], and consistent with the finding that there is a transition from dominantly pressure-driven Poiseuille flow at shorter wavelengths to dominantly shear-driven Couette flow at length scales approximately exceeding mantle depth[70,71]. With v_0 the velocity in the center of the channel at a distance d from the plume stem the total volume flux rate is $2/3 \cdot v_0 \cdot 2\pi d \cdot h_c$ (here neglecting the curvature of the Earth surface for simplicity). Its time integral is equal to the volume of the plume head with radius estimated[72] to be about r_p=500 km, with considerable uncertainty. That is, integration is done over a time interval until the entire plume head volume has flown into the asthenospheric channel. Hence the corresponding displacement vector in the center of the channel is

$$\mathbf{x}_{plu} = \int\limits_{\Delta t} v_0 dt \cdot \mathbf{e}_r = \frac{r_p^3}{d \cdot h_c} \cdot \mathbf{e}_r$$

where $\mathbf{e}_r$ is the unit vector radially away from the plume (red arrows in Extended DataFig. 1). Because of the parabolic flow profile, the vertical displacement gradient at the top of the channel is

$$2 \cdot \frac{\mathbf{x}_{plu}}{0.5 \cdot h_c} = 2 \cdot \int\limits_{\Delta t} v_0 dt \cdot \frac{1}{0.5 \cdot h_c} \cdot \mathbf{e}_r = \frac{4 r_p^3}{d \cdot h_c^2} \cdot \mathbf{e}_r.$$

Viscosity is defined such that the force per area is equal to viscosity times the radial gradient of horizontal velocity. Hence the time integral of torque on the plate is

$$\mathbf{T}_{plu} = \frac{4\eta_0}{h_c} \int\limits_{A} \mathbf{r} \times \mathbf{x}_{plu} dA = \frac{4\eta_0 r_p^3}{d \cdot h_c^2} \int\limits_{A} \mathbf{r} \times \mathbf{e}_r dA$$

where η_0 is viscosity in the channel and $\mathbf{r}$ is the position vector. $\mathbf{T}_{plu}$ is balanced by the time-integrated torque $\mathbf{T}_{pla}$ of the plate rotating an angle $\boldsymbol{\omega}$ over the underlying mantle. With plate displacement vectors $\mathbf{x}_{pla}= \boldsymbol{\omega}\ \mathrm{x}\ \mathbf{r}$ (black arrows in Fig. S1) we obtain

$$\mathbf{T}_{pla} = -\frac{\eta_0}{h_s}\int\limits_A \mathbf{r}\times\mathbf{x}_{pla}\,dA = -\frac{\eta_0}{h_s}\int\limits_A \mathbf{r}\times(\omega\times\mathbf{r})\,dA$$

Here h_s is an effective thickness of the layer over which shearing occurs, which is calculated below for a stratified viscosity structure, i.e. laterally homogeneous coupling of plate and mantle and which we will set equal to h_c for simplicity. Specifically, with $\mathbf{T}_x$ being the time-integrated torque acting on a plate rotating an angle ω_0 around the x-axis

$$\mathbf{T}_x = -\frac{\omega_0\eta_0}{h_s}\int\limits_A \mathbf{r}\times(\mathbf{e}_x\times\mathbf{r})\,dA,$$

and $\mathbf{T}_y$ and $\mathbf{T}_z$ defined in analogy, the torque balance equation can be written

$$\mathbf{T}_{plu} = \frac{\omega_x}{\omega_0}\cdot\mathbf{T}_x + \frac{\omega_y}{\omega_0}\cdot\mathbf{T}_y + \frac{\omega_z}{\omega_0}\cdot\mathbf{T}_z$$

ω_0 cancels out when T_x, T_y and T_z are inserted. Integrals used to compute these torques only depend on plate geometry, η_0 cancels out in the torque balance, and we can solve for the rotation angle vector $\boldsymbol{\omega}$ simply by a 3 x 3 matrix inversion. In the more general case, where we do not set h_s and h_c equal, $\boldsymbol{\omega}$ is scaled by a factor h_s/h_c.

If a plate moves over a mantle where viscosity varies with depth, then the force per area F/A should be the same at all depths, and the radial gradient of horizontal velocity $dv/dz = F/A \cdot 1/\eta(z)$. If we assume that the deep mantle is at rest (i.e. it moves slowly compared to plate motions), we further find that plate motion is

$$v_0 = \int\limits_{z_0}^{z(\eta_{\max})} \frac{dv}{dz}dt = \frac{F}{A}\int\limits_{z_0}^{z(\eta_{\max})} \frac{1}{\eta(z)}dz =: \frac{F}{A}\frac{h_s}{\eta_0} \tag{1}$$

The integration is done from the base of the lithosphere z_0 to the depth where the approximation of the “mantle at rest” is probably the most closely matched, i.e. we choose the viscosity maximum. The last equality is according to the definition of the effective layer thickness, whereby η_0 is the viscosity just below the lithosphere. Solving this equation for h_s for the viscosity structure in Extended DataFig. 2 and a 100 km thick lithosphere gives h_s=203.37 km.

The plume location at 27.1°E, 40.4° S, is obtained by rotating the center of the corresponding LIP at 46° E, 26° S and an age 87 Ma (adopted from Doubrovine et al.[73]) in the slab-fitted mantle reference frame[45], in which also the plate geometries at 105 Ma are reconstructed.

Results for this case (Fig. 2A) show that a plume pushing one part of a plate may induce a rotation of that plate, such that other parts of that plate may move in the opposite direction. A simple analog is a sheet of paper pushed, near its bottom left corner, to the right: Then, near the top left corner, the sheet will move to the left. With two sheets (plates) on either side, local divergence near the bottom (near the plume) may turn into convergence near the top (at the part of the plate boundary furthest away from the plume). The length of that part of the plate boundary, where convergence is induced may increase, if one plate is nearly "pinned" at a hinge point slightly NE of the plume, perhaps due to much stronger coupling between plate and mantle. At the times considered here ~105 My ago, the Indian continent, where coupling was presumably stronger, was in the southern part of the Indian plate, whereas in its north, there was a large oceanic part, with presumably weaker coupling. Hence the geometry was indeed such that convergence could be induced along a longer part of the plate boundary.

In the second case, we therefore consider lateral variations in the coupling between plate and mantle, corresponding to variations in lithosphere thickness and/or asthenosphere viscosity, by multiplying the drag force (from the first case) at each location with a resistance factor. This factor is a function of lithosphere thickness reconstructed at 105 Ma. On continents, thickness derived from tomography[74] with slabs removed[75] is simply backward-rotated. In the oceans, we use thickness [km] = $10 \cdot (\text{age [Ma]} - 105)^{0.5}$ with ages from present-day Earthbyte age grid version 3.6, i.e. accounting for the younger age and reduced thickness at 105 Ma, besides backward-rotating. To determine the appropriate rotation, the lithosphere (in present-day location) is divided up into India, Africa, Arabia, Somalia and Madagascar (paleo-)plates and respective 105 Ma finite rotations from van der Meer et al.[45] are applied. For the parts of the reconstructed plates where thickness could not be reconstructed in this way – often, because this part of the plate has been subducted – we first extrapolate thickness up to a distance ~2.3°, and set the thickness to a default value of 80 km for the remaining part. Reconstructed thickness is shown in Extended DataFig. 4. For the resistance factor as a function of lithosphere thickness we use two models: Firstly, we use a continuous curve (Extended DataFig. 3) according to eq. (1)

$$\frac{F}{A} = \frac{v_0}{\int\limits_{z_0}^{z(\eta_{\max})} \frac{1}{\eta(z)} dz}. \qquad (2)$$

with the mantle viscosity model in Extended DataFig. 2 combined with variable lithosphere thickness z_0. However, this causes only a minor change in the plate rotations (Extended DataFig. 4 compared to Fig. 2B). Hence, we also use a stronger variation, further explained in the caption of Fig 2 and with results shown in Fig. 2C and D.

Data availability

GPlates files with reconstructions used to draft Figure 1 are provided at https://figshare.com/articles/dataset/van_Hinsbergen_NatureGeo_2021_GPlates_zip/13516727.

Code availability

All codes used in the geodynamic modeling in this study are available at https://figshare.com/articles/software/van_Hinsbergen_etal_NatureGeo_2021_geodynamics_package/13635089.

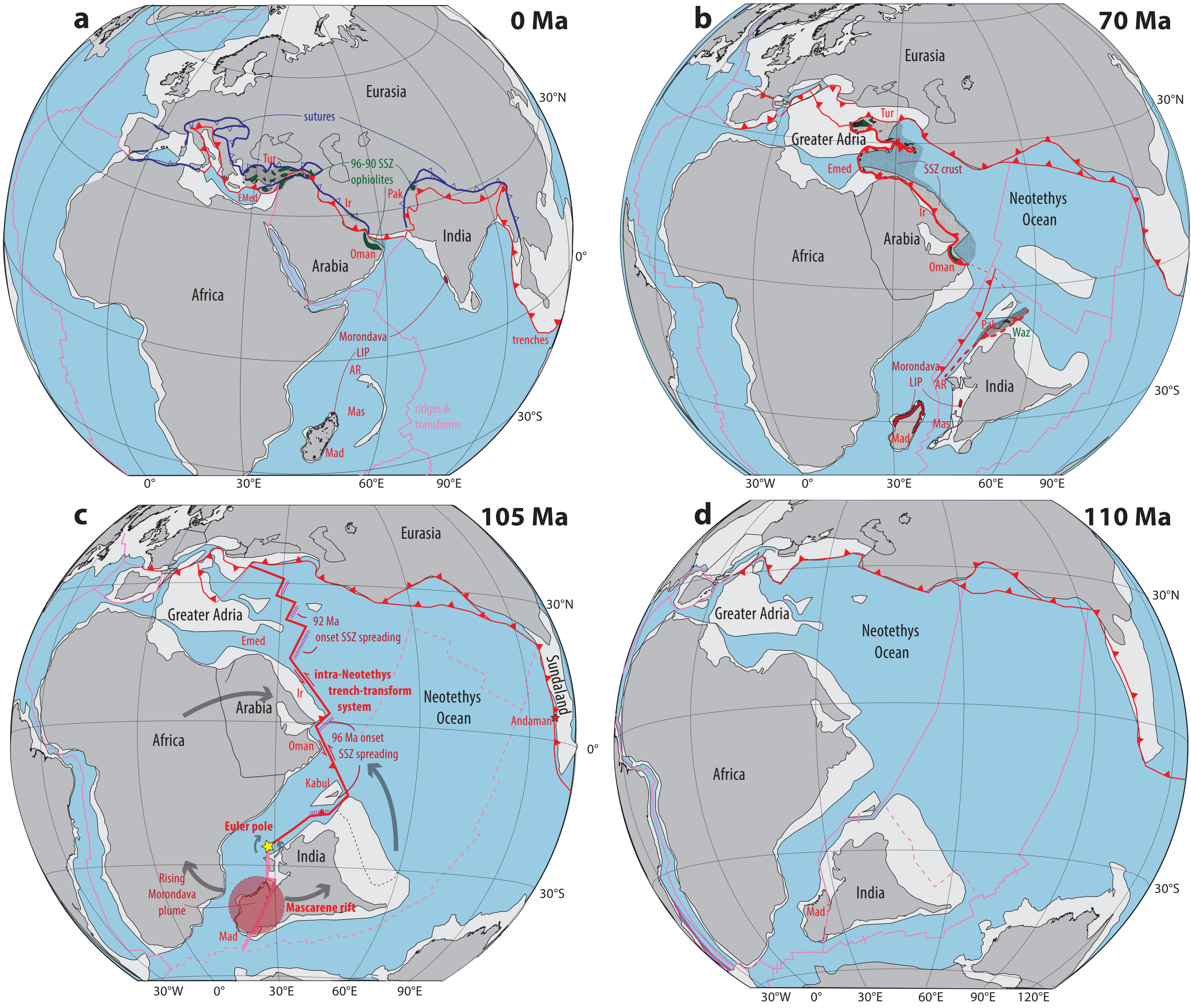
a
0 Ma
Eurasia
30°N
sutures
Tur
96-90 SSZ
ophiolites
Pak
Ir
EMed
Oman
India
Arabia
0°
Africa
Morondava
LIP
AR
trenches
Mas
ridges &
transforms
30°S
Mad
0°
30°E
60°E
90°E
b
70 Ma
Eurasia
30°N
Tur
Greater Adria
Emed
SSZ crust
Neotethys
Ocean
Ir
Arabia
Africa
0°
Oman
Pak
Waz
Morondava
LIP
AR
India
30°S
Mas
Mad
30°W
0°
30°E
60°E
90°E
c
105 Ma
Eurasia
30°N
Greater Adria
92 Ma
onset SSZ spreading
Emed
intra-Neotethys
trench-transform
system
Sundaland
Neotethys
Ocean
Arabia
Ir
Africa
Andaman
0°
Oman
96 Ma onset
SSZ spreading
Kabul
Euler pole
India
Rising
Morondava
plume
30°S
Mascarene rift
Mad
30°W
0°
30°E
60°E
90°E
d
110 Ma
30°N
Greater Adria
Neotethys
Ocean
Africa
0°
India
Mad
30°S
30°W
0°
30°E
60°E
90°E
120°E

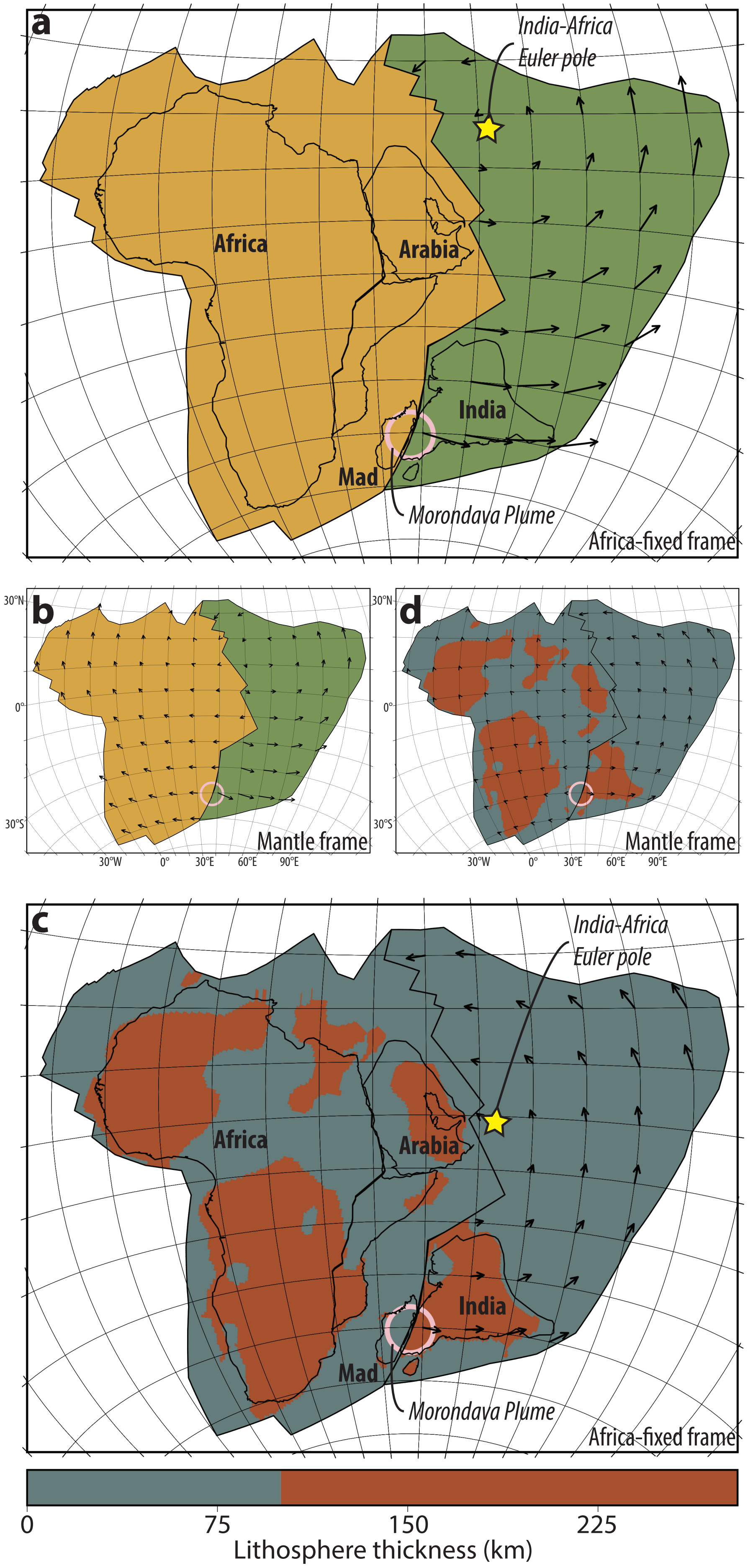
a
India-Africa
Euler pole
Africa
Arabia
India
Mad
Morondava Plume
Africa-fixed frame
b
30°N
0°
30°S
30°W
0°
30°E
60°E
90°E
Mantle frame
d
30°N
0°
30°S
30°W
0°
30°E
60°E
90°E
Mantle frame
c
India-Africa
Euler pole
Africa
Arabia
India
Mad
Morondava Plume
Africa-fixed frame
0
75
150
225
Lithosphere thickness (km)

Extended Data

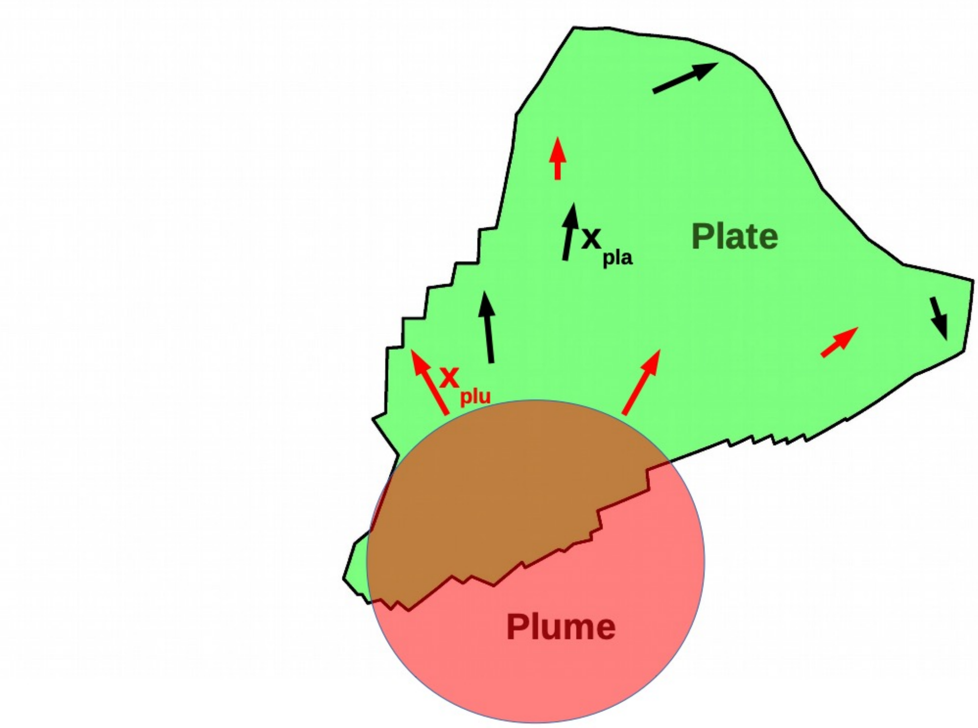

Extended Data Fig. 1: Sketch illustrating the geometry of a plume head (pink; not drawn to scale) hitting the boundary of a plate (green). x_{plu} (red arrows) are the (maximum) displacement vectors in the asthenosphere caused by emplacement of the plume. Motion vectors of the plate x_{pla} (black arrows) correspond to the plate rotation $\boldsymbol{\omega}$ that is caused. Reversal of direction from left to right indicates the rotational component of motion induced by the plume push. Note that, since plume push is modelled as Poiseuille flow, the red arrows correspond to flow in the mid-asthenosphere, whereas plate motions induce Couette-type flow, therefore are shown at lithosphere depth.

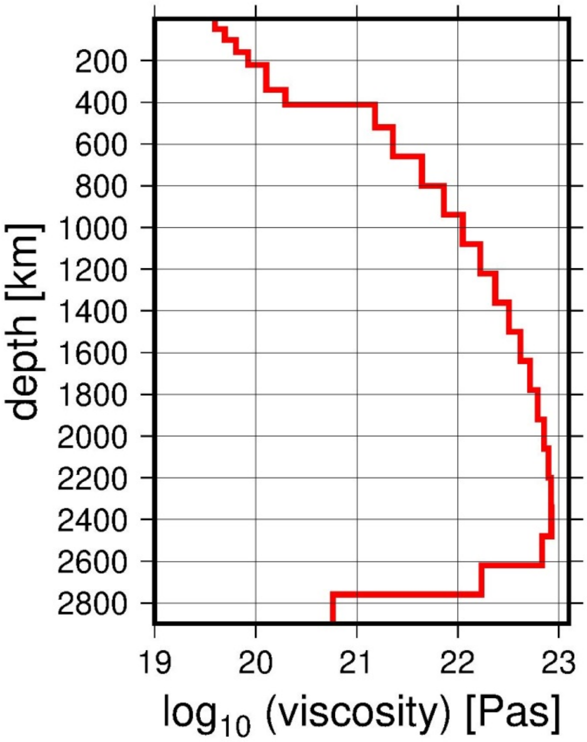

Extended Data Fig. 2: Viscosity structure used, similar to Steinberger[66]but without lithosphere. This is being combined with a lithosphere of constant or variable thickness.

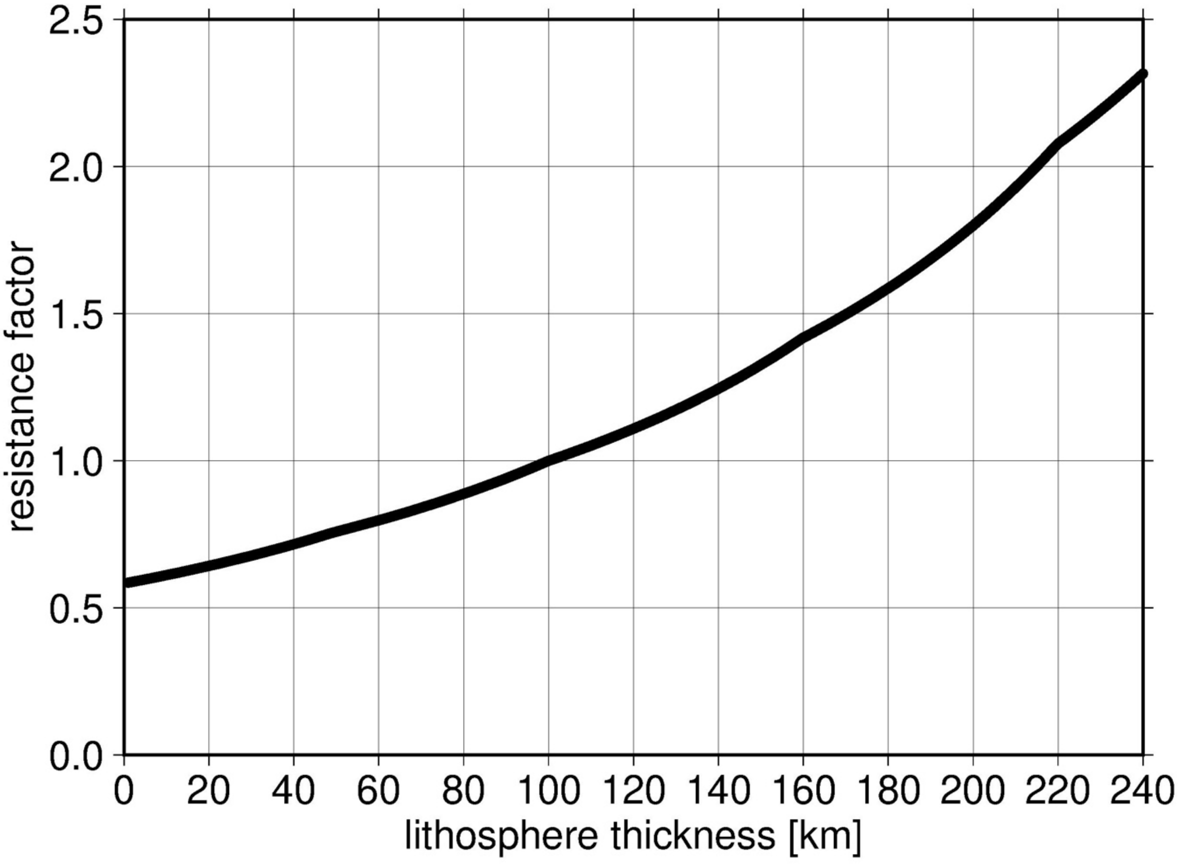

Extended Data Fig. 3: Resistance factor to account for laterally variable coupling between lithosphere and mantle as a function of lithosphere thickness, for sub-lithospheric viscosity as in Fig. S2, according to eq. (2).

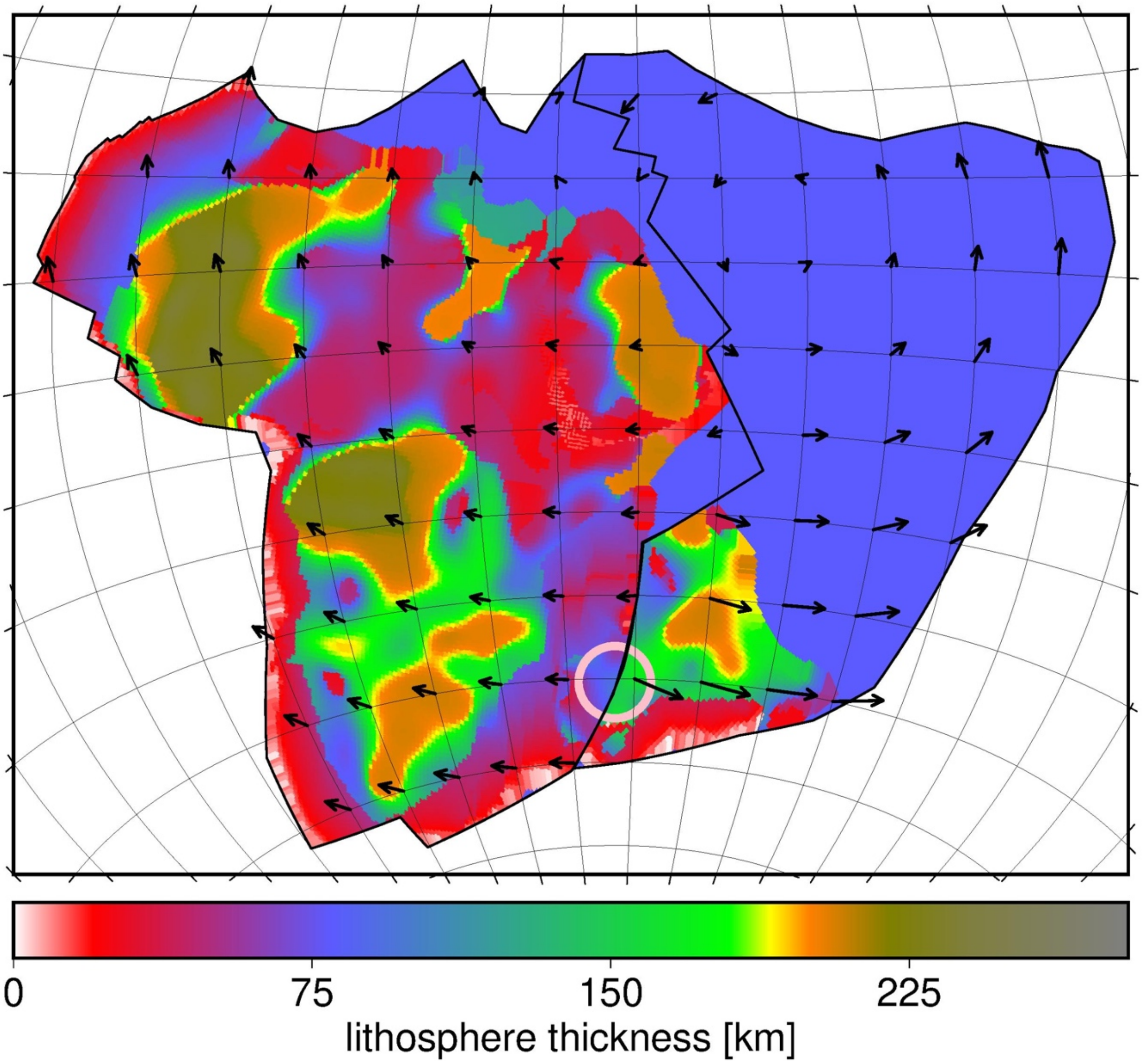

Extended Data Fig. 4: Computed total amount of displacement induced by the Morondava plume (pink circle), considering lithosphere thickness variations: It is assumed that, compared to a case with no lateral variations, the drag force due to the plate moving over the mantle is multiplied at each location with a resistance factor according to Fig. S3. Plates, plume and lithosphere thickness are reconstructed in the slab-fitted mantle reference frame[46].